

Table S1 Results of Pawley and Rietveld fits of synchrotron X-ray data for nominal  $\text{La}_8\text{Sr}_2(\text{GeO}_4)_6\text{O}_2$ .

# Phases	Space-group phase #1	Space-group phase #2	Pawley fits		Rietveld fits	
			$R_{\text{wp}}/R_{\text{Bp1}}/R_{\text{Bp2}}^\dagger$		$R_{\text{wp}}/R_{\text{Bp1}}/R_{\text{Bp2}}^\dagger$	
1	$P6_3/m$	-	20.0 / 5.7		22.1 / 8.0	
1	$P2_1/m$	-	13.0 / 1.5		18.2 / 7.9	
1	$P\bar{1}$	-	11.4 / 1.1		16.6 / 7.4	
2	$P6_3/m$	$P6_3/m$	14.7 / 2.7 / 1.4		18.4 / 8.1 / 7.6	
2	$P6_3/m$	$P2_1/m$	10.8 / 2.6 / 0.7		15.1 / 6.7 / 7.6	
2	$P6_3/m$	$P\bar{1}$	10.2 / 1.9 / 0.7		14.5 / 8.3 / 7.6	
2	$P2_1/m$	$P2_1/m$	9.9 / 0.9 / 0.6		12.9 / 6.5 / 7.0	
2	$P2_1/m$	$P\bar{1}$	9.8 / 0.8 / 0.9		14.0 / 6.8 / 7.2	
2	$P\bar{1}$	$P\bar{1}$	9.6 / 0.7 / 0.5		13.9 / 7.4 / 6.7	

<sup>†</sup> Agreement measures are  $R_{\text{wp}} = [(\sum_i w_i |y_{io} - y_{ci}|^2) / \sum_i w_i y_{io}^2]^{1/2}$  and  $R_{\text{B}} = \sum_i |I_{ko} - I_{kc}| / \sum_i I_{ko}$ . p1 and p2 are for phase #1 and phase #2 respectively.

Table S2 Selected bond lengths of the average  $[\text{La}_8\text{Sr}_2][(\text{GeO}_4)_6]\text{O}_2$ .

	phase #1	phase #2
La/Sr1–O1	2.534(7)	2.536(7)
La/Sr1–O2	2.472(10)	2.474(10)
La/Sr1–O3	2.460(8)	2.462(8)
La/Sr1–O4	2.570(16)	2.573(16)
La/Sr1–O5	2.599(16)	2.601(16)
La/Sr1–O6	2.623(6)	2.626(6)
La/Sr1–O7	2.885(14)	2.886(14)
La/Sr1–O8	2.891(6)	2.893(6)
La/Sr1–O9	3.131(16)	3.134(16)
Average	2.685	2.687
La2–O2	2.788(19)	2.791(19)
La2–O6	2.480(9)	2.481(9)
La2–O7 [x 2]	2.651(8)	2.654(8)
La2–O9 [x 2]	2.431(8)	2.434(8)
La2–O10	2.319(8)	2.320(8)
Average	2.536	2.538
La3–O3	2.880(19)	2.882(19)
La3–O4	2.526(19)	2.529(19)
La3–O7 [x 2]	2.469(9)	2.471(9)
La3–O8 [x 2]	2.657(9)	2.660(9)
La3–O10	2.304(8)	2.306(8)
Average	2.566	2.568
La4–O1	2.651(7)	2.653(7)
La4–O5	2.478(21)	2.480(21)
La4–O8 [x 2]	2.445(7)	2.447(7)
La4–O9 [x 2]	2.592(7)	2.594(7)
La4–O10	2.412(8)	2.414(8)
Average	2.516	2.518
Ge1–O1	1.726(12)	1.727(12)
Ge1–O4	1.744(9)	1.746(9)
Ge1–O7 [x 2]	1.740(8)	1.742(8)
Average	1.738	1.739
Ge2–O2	1.724(9)	1.725(9)
Ge2–O5	1.740(10)	1.742(10)
Ge2–O8 [x 2]	1.737(8)	1.738(8)
Average	1.735	1.736
Ge3–O3	1.723(9)	1.724(9)
Ge3–O6	1.743(13)	1.744(13)
Ge3–O9 [x 2]	1.738(8)	1.739(8)
Average	1.736	1.737

Table S3 Selected bond lengths of  $[\text{La}_{10-x}\text{Sr}_x][(\text{GeO}_4)_6]\text{O}_2\text{H}_8$  ( $2.96 \leq x \leq 5.32$ ).

	$x = 2.96$	$x = 3.54$	$x = 4.48$	$x = 5.32$
La/Sr1–O1 [x 3]	2.497(8)	2.517(11)	2.506(9)	2.503(11)
La/Sr1–O2 [x 3]	2.574(9)	2.568(12)	2.580(11)	2.576(16)
La/Sr1–O3 [x 3]	2.956(8)	2.957(9)	2.977(9)	2.976(11)
Average	2.676	2.681	2.688	2.685
La/Sr2–O1	2.732(8)	2.727(8)	2.704(10)	2.719(11)
La/Sr2–O2	2.504(9)	2.494(12)	2.493(13)	2.501(17)
La/Sr2–O3 [x 2]	2.448(6)	2.461(7)	2.457(7)	2.456(10)
La/Sr2–O3 [x 2]	2.625(7)	2.615(10)	2.615(9)	2.632(14)
La/Sr2–O4	2.406(4)	2.431(9)	2.461(8)	2.503(13)
Average	2.541	2.543	2.543	2.557
Ge1-O1	1.749(13)	1.746(14)	1.742(17)	1.741(20)
Ge1-O2	1.753(10)	1.762(11)	1.754(13)	1.761(16)
Ge1-O3 [x 2]	1.740(6)	1.733(7)	1.747(7)	1.733(9)
Average	1.746	1.744	1.748	1.742
O4-O4	0.56(5)	0.67(4)	0.69(5)	0.68(7)
O4-H1	1.20(7)	1.30(18)	1.49	1.51

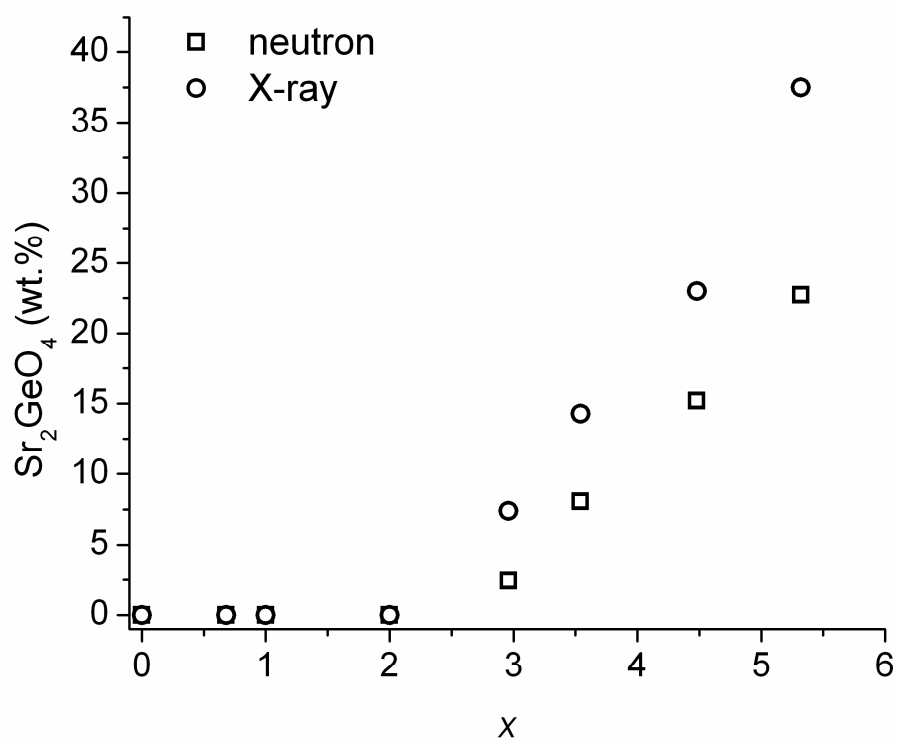


Fig. S1 Second phase  $\text{Sr}_2\text{GeO}_4$  formed as a function of  $x$

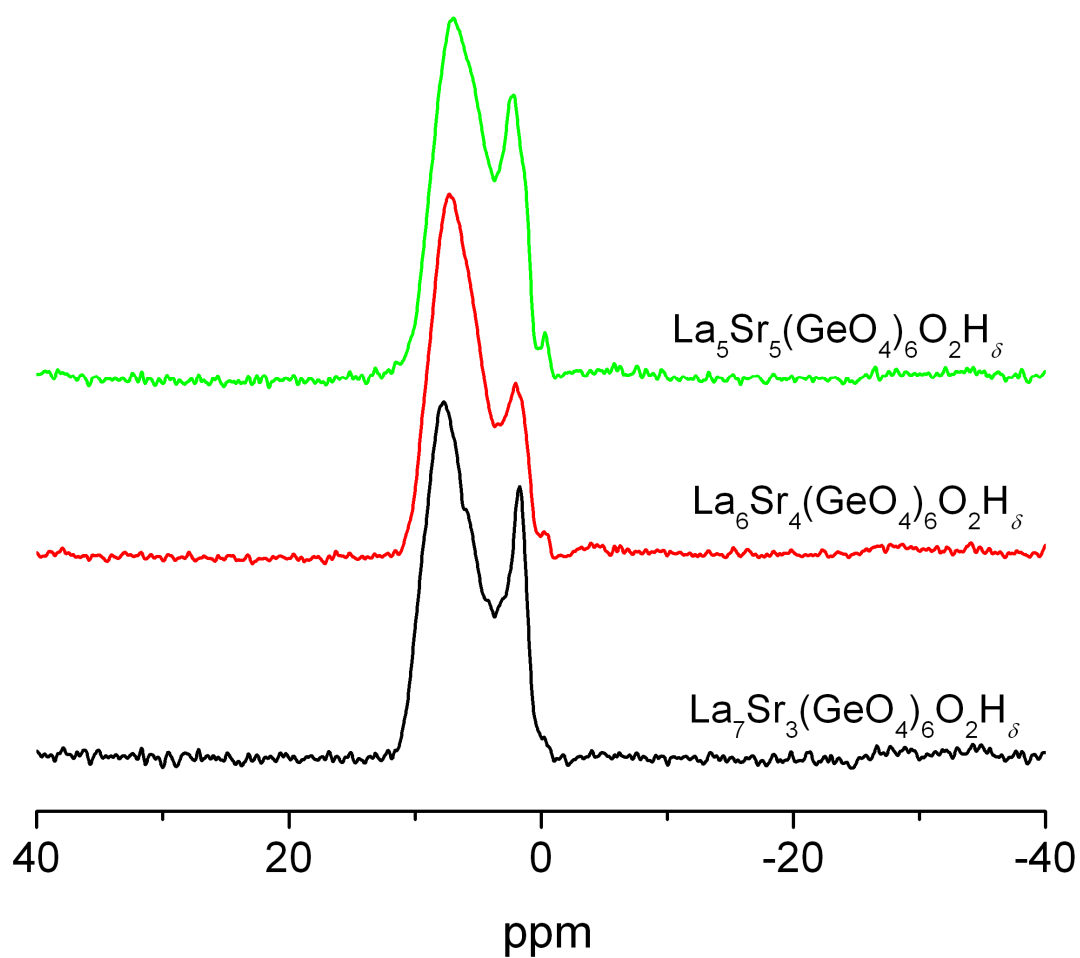


Fig. S2 Solid state  $^1\text{H}$  NMR data of nominal  $\text{La}_7\text{Sr}_3$ ,  $\text{La}_6\text{Sr}_4$ , and  $\text{La}_5\text{Sr}_5\text{Ge}_6\text{O}_{26}\text{H}_\delta$ .

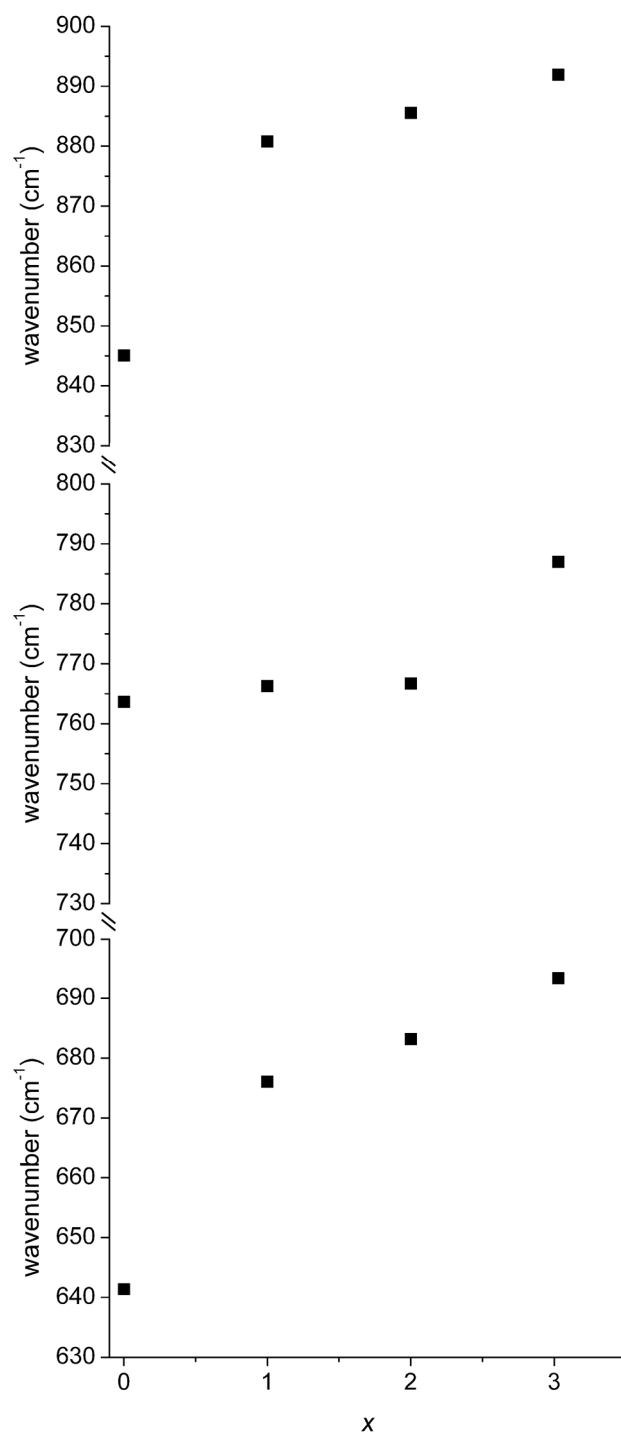


Fig. S3 IR wavenumber shift trends with different Sr composition.

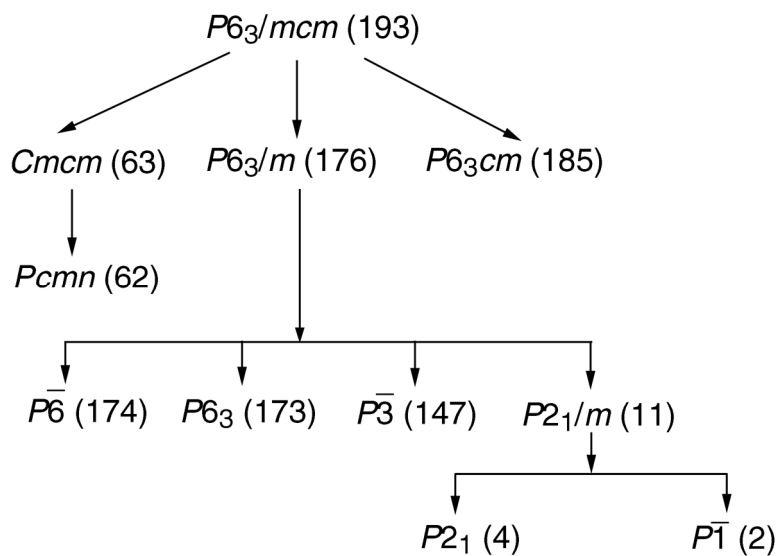


Fig. S4 Symmetry relationships for apatite hettotypes [Adapted from Schriewer & Jeitschko (1993)<sup>67</sup> and White & Dong (2003)<sup>8</sup>].

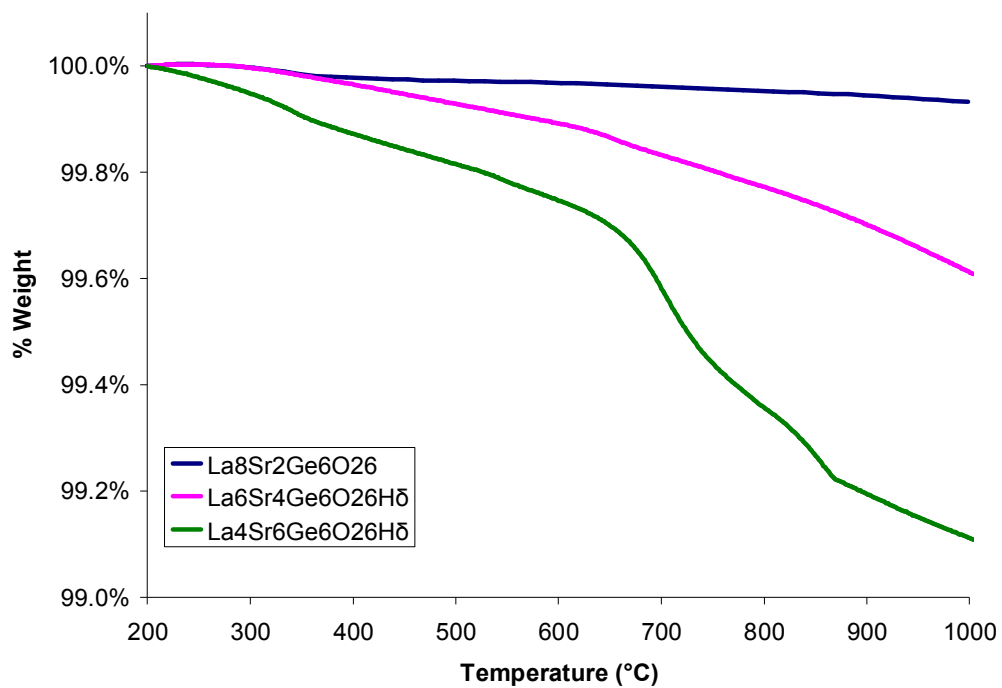


Fig. S5 TGA plots for nominal  $\text{La}_8\text{Sr}_2\text{Ge}_6\text{O}_{26}$ ,  $\text{La}_6\text{Sr}_4\text{Ge}_6\text{O}_{26}\text{H}_\delta$ , and  $\text{La}_4\text{Sr}_6\text{Ge}_6\text{O}_{26}\text{H}_\delta$ .



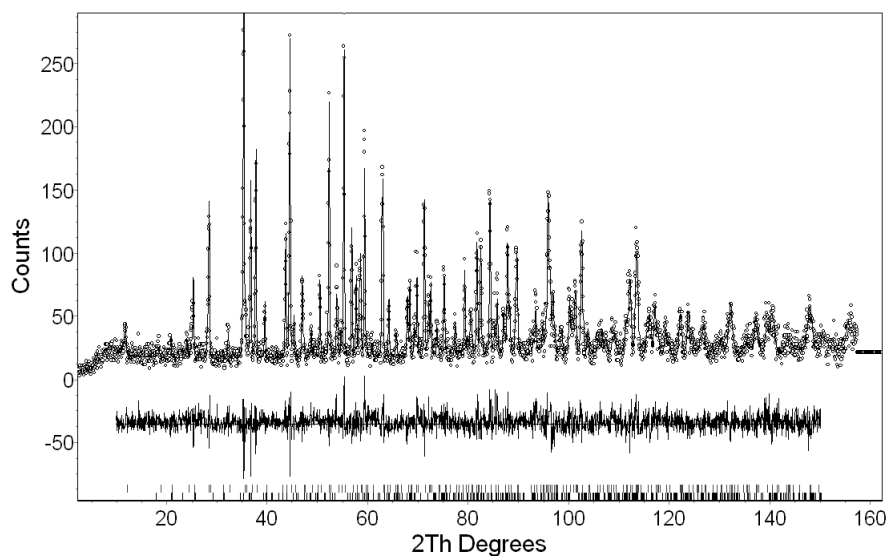


Figure S6 Rietveld plot of the neutron diffraction data of  $\text{La}_{7.04}\text{Sr}_{2.96}\text{Ge}_6\text{O}_{26}\text{H}_{0.96}$  collected at room temperature. The observed intensity data are shown by dots, with the solid line representing the calculated intensity. Differences between observed and calculated intensities are plotted beneath. Vertical markers indicate the Bragg reflections of apatite (top) and  $\text{Sr}_2\text{GeO}_4$  phases (bottom).

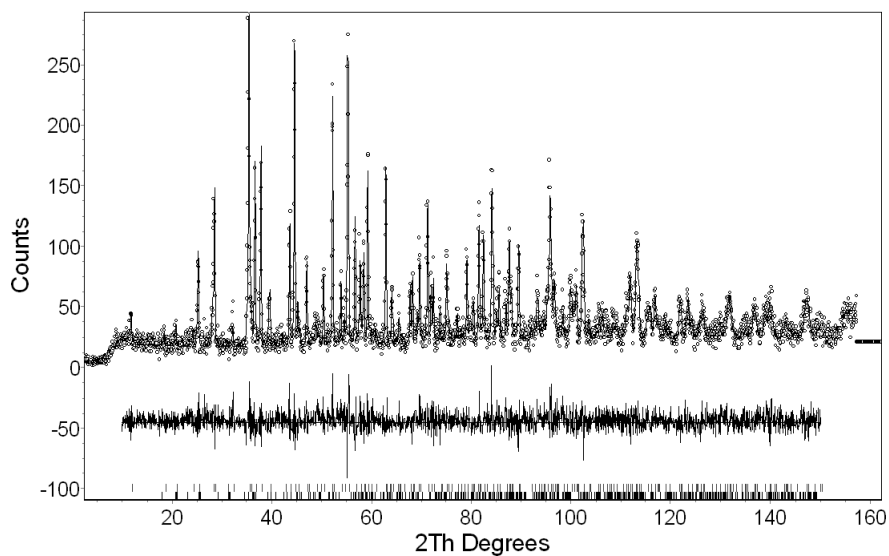


Figure S7 Rietveld plot of the neutron diffraction data of  $\text{La}_{6.46}\text{Sr}_{3.54}\text{Ge}_6\text{O}_{26}\text{H}_{1.54}$  collected at room temperature. The observed intensity data are shown by dots, with the solid line representing the calculated intensity. Differences between observed and calculated intensities are plotted beneath. Vertical markers indicate the Bragg reflections of apatite (top) and  $\text{Sr}_2\text{GeO}_4$  phases (bottom).

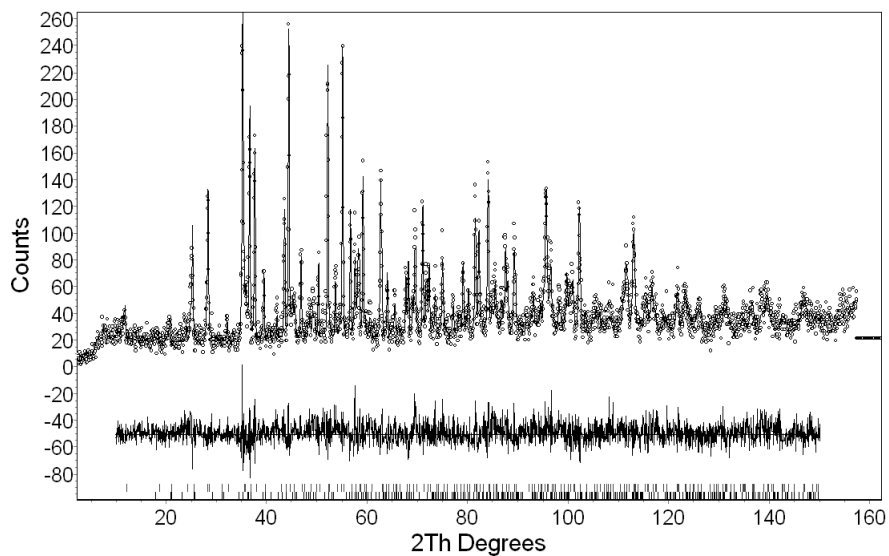


Figure S8 Rietveld plot of the neutron diffraction data of  $\text{La}_{5.52}\text{Sr}_{4.48}\text{Ge}_6\text{O}_{26}\text{H}_{2.48}$  collected at room temperature. The observed intensity data are shown by dots, with the solid line representing the calculated intensity. Differences between observed and calculated intensities are plotted beneath. Vertical markers indicate the Bragg reflections of apatite (top) and  $\text{Sr}_2\text{GeO}_4$  phases (bottom).

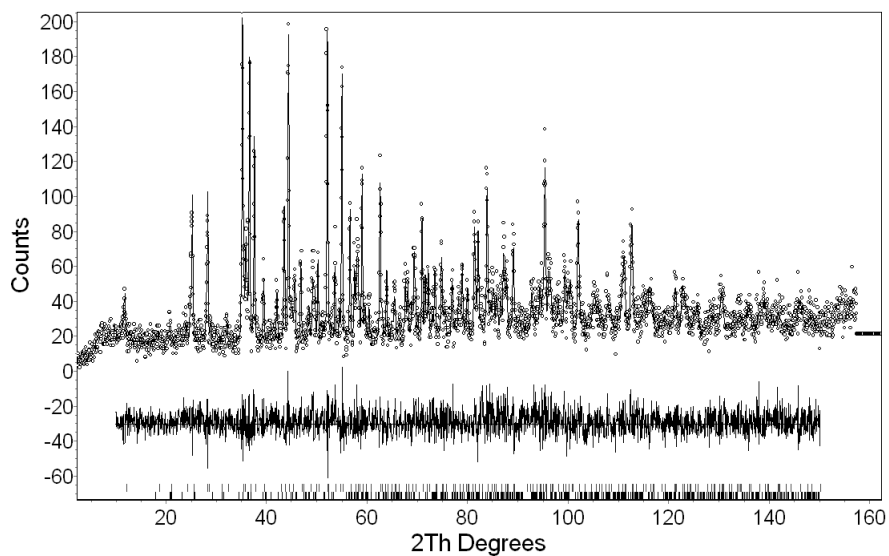


Figure S9 Rietveld plot of the neutron diffraction data of  $\text{La}_{4.68}\text{Sr}_{5.32}\text{Ge}_6\text{O}_{26}\text{H}_{3.32}$  collected at room temperature. The observed intensity data are shown by dots, with the solid line representing the calculated intensity. Differences between observed and calculated intensities are plotted beneath. Vertical markers indicate the Bragg reflections of apatite (top) and  $\text{Sr}_2\text{GeO}_4$  phases (bottom).